Available online at www.sciencedirect.com
ScienceDirect
Matrix Biology 26 (2007) 442–455
MATRIX BIOLOGY
www.elsevier.com/locate/matbio

The principal neuronal gD-type 3-*O*-sulfotransferases and their products in central and peripheral nervous system tissues☆

Roger Lawrence [a,1,2], Tomio Yabe [b,1,3], Sassan HajMohammadi [c], John Rhodes [c], Melissa McNeely [d], Jian Liu [e], Edward D. Lamperti [f], Paul A. Toselli [f], Miroslaw Lech [a], Patricia G. Spear [d], Robert D. Rosenberg [a], Nicholas W. Shworak [c,*]

[a] *Department of Biology, Massachusetts Institute of Technology, Cambridge, MA 02139, United States*
[b] *Department Chemistry, Massachusetts Institute of Technology, Cambridge, MA 02139, United States*
[c] *Department of Medicine , Dartmouth Medical School, Hanover, NH 03756, United States*
[d] *Department of Microbiology-Immunology, Feinberg School of Medicine, Northwestern University, Chicago, IL , United States*
[e] *Department of Medicinal Chemistry and Natural Products, University of North Carolina, Chapel Hill, NC, United States*
[f] *Department of Biochemistry, Boston University School of Medicine, Boston, MA 02118, United States*

Received 1 February 2007; received in revised form 19 March 2007; accepted 20 March 2007

Abstract

Within the nervous system, heparan sulfate (HS) of the cell surface and extracellular matrix influences developmental, physiologic and pathologic processes. HS is a functionally diverse polysaccharide that employs motifs of sulfate groups to selectively bind and modulate various effector proteins. Specific HS activities are modulated by 3-*O*-sulfated glucosamine residues, which are generated by a family of seven 3-*O*-sulfotransferases (3-OSTs). Most isoforms we herein designate as gD-type 3-OSTs because they generate HS^{gD+}, 3-*O*-sulfated motifs that bind the gD envelope protein of herpes simplex virus 1 (HSV-1) and thereby mediate viral cellular entry. Certain gD-type isoforms are anticipated to modulate neurobiologic events because a *Drosophila* gD-type 3-OST is essential for a conserved neurogenic signaling pathway regulated by Notch. Information about 3-OST isoforms expressed in the nervous system of mammals is incomplete. Here, we identify the 3-OST isoforms having properties compatible with their participation in neurobiologic events. We show that 3-OST-2 and 3-OST-4 are principal isoforms of brain. We find these are gD-type enzymes, as they produce products similar to a prototypical gD-type isoform, and they can modify HS to generate receptors for HSV-1 entry into cells. Therefore, 3-OST-2 and 3-OST-4 catalyze modifications similar or identical to those made by the *Drosophila* gD-type 3-OST that has a role in regulating Notch signaling. We also find that 3-OST-2 and 3-OST-4 are the predominant isoforms expressed in neurons of the trigeminal ganglion, and 3-OST-2/4-type 3-*O*-sulfated residues occur in this ganglion and in select brain regions. Thus, 3-OST-2 and 3-OST-4 are the major neural gD-type 3-OSTs, and so are prime candidates for participating in HS-dependent neurobiologic events.

Keywords: Heparan sulfate proteoglycan; 3-*O*-sulfotransferase; Brain; Herpes simplex virus; gD

☆ The nucleotide sequence(s) reported in this paper has been submitted to the GenBankTM/EBI Data Bank with accession number(s) AY476736 and AF105378.

* Corresponding author. Angiogenesis Research Center, Section of Cardiology, Borwell Building 540W, HB7504, Dartmouth-Hitchcock Medical Center, One Medical Center Drive, Lebanon, NH 03756, United States. Tel.: +1 603 650 6401; fax: +1 603 653 0510.
E-mail address: nicholas.shworak@dartmouth.edu (N.W. Shworak).
[1] These authors contributed equally to this work.
[2] Present address: University of California San Diego, La Jolla, CA, United States.
[3] Present address: Applied Biological Sciences, Gifu University, Gifu 501-1193, Japan.

0945-053X/$ - see front matter
doi:10.1016/j.matbio.2007.03.002

1. Introduction

Heparan sulfate (HS)[4] is expressed by the majority of mammalian cell-types as side chains on cell surface and extracellular matrix proteoglycans that regulate numerous biological pathways (Gallagher, 2001; Iozzo and San Antonio, 2001; Rosenberg et al., 1997; Sasisekharan et al., 2002). Within the nervous system, HS influences such developmental processes as neurogenesis and differentiation, axon branching and guidance, and synaptogenesis (Bulow et al., 2002; Chipperfield et al., 2002; Ford-Perriss et al., 2002; Grobe et al., 2005; Inatani et al., 2003; Irie et al., 2002; Kamimura et al., 2004; Yamaguchi, 2001). In the adult, HS continues to modulate important neurologic activities such as learning and eating behavior (Kaksonen et al., 2002; Reizes et al., 2001). HS also participates in pathological events, including Alzheimer's disease (Goedert et al., 1996; Hasegawa et al., 1997; Paudel and Li, 1999).

The functional diversity of HS stems from its structural complexity, which results from its intricate pathway of biosynthesis. HS is produced as a proteoglycan (HSPG) consisting of a protein core with attached HS chains. The HS moieties are linear copolymers composed of up to 100 disaccharide units of *N*-acetylglucosamine (GlcNAc) $\alpha 1 \rightarrow 4$ glucuronic/iduronic acid (GlcA/IdoA) $\beta/\alpha 1 \rightarrow 4$. Structural heterogeneity arises from the remodeling of the copolymer backbone by a relatively ordered series of reactions involving an epimerase and four families of sulfotransferases (reviewed by Esko and Lindahl, 2001; Iozzo, 2001). The sulfotransferases differentially place *N*- and *O*-sulfate groups within HS. The arrangement of these critical groups along the HS chain creates distinct binding motifs that can activate an array of important effector proteins.

3-*O*-Sulfation of glucosamine residues is a key regulator of discrete HS activities. The activities of several effectors are influenced by selective binding to 3-*O*-sulfated HS motifs. The best characterized interaction involves the antithrombin-binding site, which accelerates antithrombin neutralization of proteases of the blood coagulation cascade (Shworak and Rosenberg, 1995). Additionally, 3-*O*-sulfated HS has been found to bind to fibroblast growth factor 7, to a receptor for fibroblast growth factors, and to the envelope glycoprotein D (gD) of herpes simplex virus type 1 (HSV-1) (Liu et al., 1996; McKeehan et al., 1999; Shukla et al., 1999; Ye et al., 2001). Biosynthesis of discrete 3-*O*-sulfated motifs is controlled by distinct forms of HS 3-*O*-sulfotransferase (3-OST). Indeed, 3-OSTs comprise the largest multigene family of HS biosynthetic enzymes, with a total of seven different 3-OST isoforms having been identified (Daniels et al., 2001; Shworak et al., 1999; Xia et al., 2002).

All 3-OSTs exhibit a conserved C-terminal sulfotransferase domain, which determines enzymatic sequence specificity such that isoforms preferentially generate a subset of 3-*O*-sulfated motifs (Shworak et al., 1999; Yabe et al., 2001). 3-OST-1 principally creates HS with antithrombin-binding sites (HS^{AT+}); 3-OST-3_A, 3-OST-3_B, and 3-OST-6 primarily generate HS with gD-binding sites (HS^{gD+}); and 3-OST-5 efficiently produces both HS^{AT+} and HS^{gD+} (Liu et al., 1999b; Shukla et al., 1999; Xia et al., 2002; Xu et al., 2005; Yabe et al., 2001). These enzymes, with their distinct substrate specificities, are ideally suited to regulate biologic activities of HS as (1) 3-*O*-sulfates are the rarest HS modifications, (2) 3-OSTs act very late in HS biosynthesis, (3) 3-OST activity can be rate-limiting to control the cellular level of 3-*O*-sulfated motifs, and (4) the large multiplicity of genes allows tremendous regulatory flexibility with individual isoforms exhibiting cell-type, tissue-specific, and temporal regulation (Borjigin et al., 2003; Colliec-Jouault et al., 1994; Kamimura et al., 2004; Kuberan et al., 2004; Shworak et al., 1994a, 1996, 1997; Shworak, 2001).

3-OSTs are expected to modulate neurobiologic processes, as a *Drosophila* 3-OST isoform regulates Notch signaling (Kamimura et al., 2004), which is an essential metazoan pathway known to control mammalian central nervous system development and function (Artavanis-Tsakonas et al., 1999; Grandbarbe et al., 2003). Indeed, several mammalian 3-OST isoforms are expressed in the brain (Mochizuki et al., 2003; Shworak et al., 1999); however, it is unknown if any of these isoforms exhibit neuronal expression. The identification of the major neuronal 3-OST isoforms would enable investigations into whether these critical regulators of HS motifs are involved in developmental, physiological, and pathological aspects of neurobiology.

HSV-1 is a major neuropathogen that potentially can exploit endogenous 3-*O*-sulfated HS for entry into neurons or for other aspects of the infection process (Shukla and Spear, 2001). Viral entry is triggered by interactions between glycoprotein gD and any one of several cell surface components (Spear et al., 2000), including HS^{gD+} (Liu et al., 2002; Shukla et al., 1999; Xu et al., 2005; Yoon et al., 2003). Evidence has been presented that another HSV-1 receptor, nectin-1, can mediate the entry of the virus into cultured cells of neuronal origin (Manoj et al., 2004; Richart et al., 2003) but this evidence does not rule out a role for 3-*O*-sulfated HS in HSV-1 infection of neurons *in situ*. Typically, an initial HSV-1 infection can spread from mucosal or skin epithelial cells to the neurons of sensory ganglia such as the trigeminal ganglia. These neurons can then harbor latent HSV-1, which upon reactivation causes recurrent herpes (cold sores, for example). HSV-1 infection can also spread into the central nervous system, where it is the most common cause of sporadic, fatal encephalitis in the United States (reviewed by Schmutzhard, 2001).

Here, we show that 3-OST-2 and 3-OST-4 are major brain/neuronal 3-OST isoforms with properties that make them prime candidates for participating in HS-dependent neurobiologic events.

[4] The abbreviations used are as follows: HS, heparan sulfate; 3-OST, HS 3-*O*-sulfotransferase; HS^{gD+}, HS with gD-binding sites; HSV-1, herpes simplex virus 1; HSPG, HS proteoglycan; GlcNAc, *N*-acetylglucosamine; GlcA, D-glucuronic acid; IdoA, L-iduronic acid; gD, glycoprotein D; HS^{AT+}, HS with antithrombin-binding motifs; LCM, laser capture microdissection; Hep I–III, heparinase I, II, and III; LC/MS, liquid chromatography/mass spectrometry; ΔUA2S, 4,5-unsaturated uronic acid 2-*O*-sulfate; IdoA2S, L-iduronic acid 2-*O*-sulfate; GlcNS**3S**, glucosamine *N*-sulfate 3-*O*-sulfate; GlcNS**3S**6S, glucosamine *N*-sulfate 3-*O*-sulfate 6-*O*-sulfate; GlcN(S/H)**3S**±6S, glucosamine *N*-sulfate or free amino 3-*O*-sulfate with or without 6-*O*-sulfate; PBS, phosphate-buffered saline; DBA, dibutylamine.

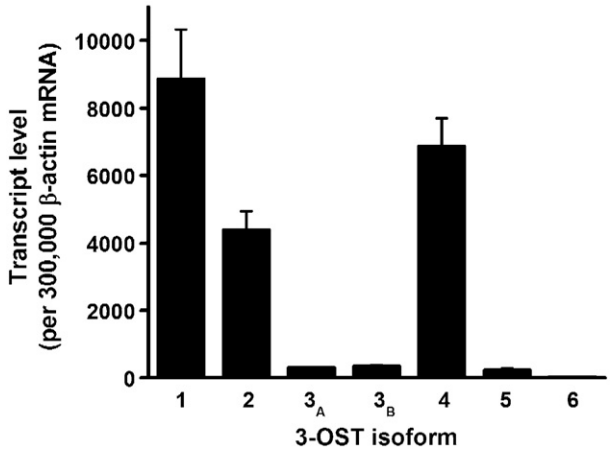

Fig. 1. Expression level of 3-OST isoforms in brain. Real-time RT-PCR of mouse brain total RNA was conducted using isoform specific primers for both first strand synthesis and PCR amplification. Transcript levels were calibrated against standard curves generated from cloned PCR products, and then standardized to the sample levels of β-actin, as described under Experimental procedures. The results are expressed as the mean ± SEM for RNA samples extracted from eight separate mouse brains. 3-OST-6 expression levels, although low, were significantly above background reactions lacking reverse transcriptase.

2. Results

2.1. Identification of major brain 3-OST isoforms

To identify 3-OST isoforms having properties compatible with their participation in neurobiologic events, we first determined the predominant 3-OST isoforms in brain. We measured the levels of transcripts from all seven 3-OST genes by real-time PCR of total RNA extracted from mouse brain. Each isoform is expressed to some degree in the brain (Fig. 1). However, 3-OST-1, 3-OST-2, and 3-OST-4 predominate with transcript levels being at least 10-fold higher than those of the remaining isoforms. We have previously determined that 3-OST-1 is principally expressed in endothelial cells (Shworak et al., 1997); whereas, 3-OST-2 and 3-OST-4 are primarily and exclusively expressed in brain, respectively (Shworak et al., 1999). Together, these data raise the possibility that 3-OST-2 and 3-OST-4 may be the major isoforms expressed in neurons.

2.2. Neurons of the trigeminal ganglion express 3-OST-2 and 3-OST-4

We initially tested for neuronal expression by performing *in situ* hybridizations on mouse brain sections. 3-OST-2 and 3-OST-

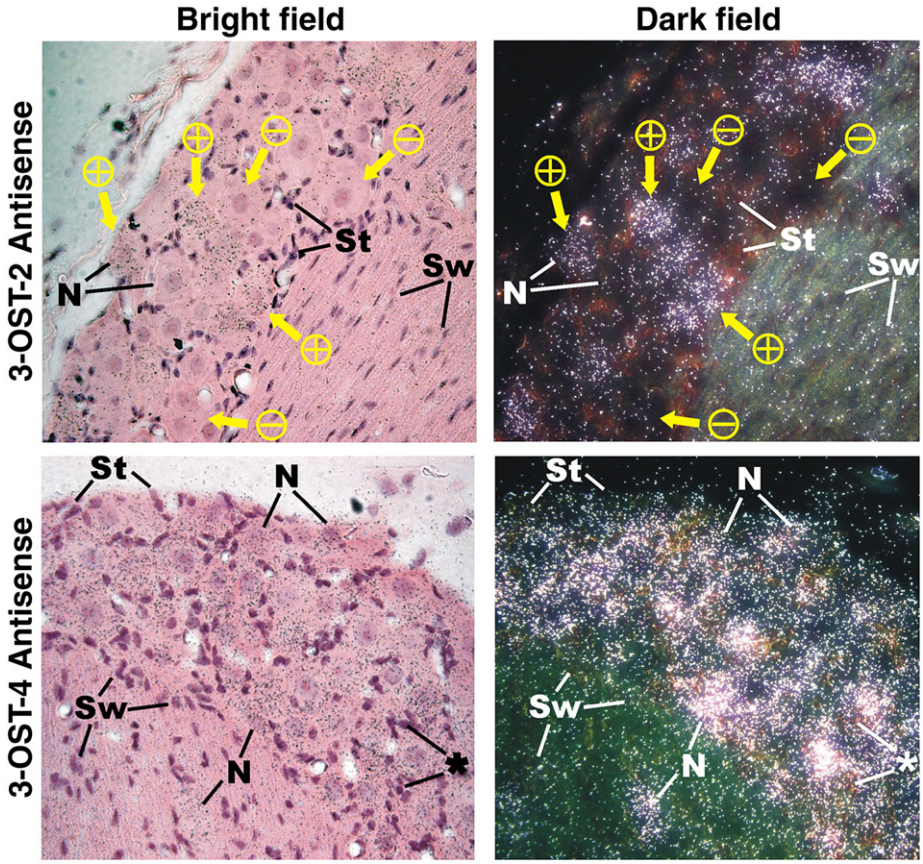

Fig. 2. Neuronal expression of 3-OST-2 and 3-OST-4 in the mouse trigeminal ganglia. *In situ* hybridizations with 3-OST-2 or 3-OST-4 antisense probes, as indicated, were performed on trigeminal ganglia longitudinal sections. Hybridization signals are most evident in the dark field images, seen as white grains. The corresponding hematoxylin/eosin stained bright field images show sensory ganglion cell bodies (upper portion of images) and an adjacent axon bundle (lower portion of images). Representative neurons (N), satellite cells (St), and Schwann cells (Sw) are indicated in these 400× images. For the 3-OST-2 probe, only scattered neurons exhibited significant hybridization signals (+). The remaining neurons (-) and non-neuronal cells exhibited a silver grain density that was comparable to control hybridizations with a sense probe (not shown). The 3-OST-4 signal is especially conspicuous over the majority of neuronal cell bodies. Reduced yet significant signal is also evident over satellite cells adjacent to highly expressive neurons (*). Silver grain density over axons was comparable to the background of the 3-OST-4 control sense probe (not shown).

4 mRNAs exhibited distinct patterns of expression in subsets of neurons in multiple brain regions. These neuronal expression patterns were extremely complex and so shall be elaborated upon in a separate publication.[5] Here, we describe their expression in the mouse trigeminal ganglion, which exhibits abundant sensory neurons with well defined projections.

For both 3-OST-2 and 3-OST-4, significant hybridization signals were detected primarily in regions containing neuronal cell bodies, with individual neurons differing in the level of expression (Fig. 2). Only a subset of neurons expressed 3-OST-2, whereas 3-OST-4 expression was detected in the majority of neurons. Moreover, the 3-OST-4 hybridization signal overlapped some satellite cells that were adjacent to neurons with high expression. It is unclear, however, whether this lower signal truly originates from the satellite cells or from underlying neuronal cytoplasm within the section plane. Alternatively, this signal may simply reflect scattered radiation emanating from the highly expressive neurons. Sensitivity limitations preclude us from ruling out a low expression level of either 3-OST isoform in non-neuronal cell types. These data demonstrate that within the trigeminal ganglion, 3-OST-2, and 3-OST-4 are predominantly, if not exclusively, expressed in neurons.

2.3. Identification of major 3-OST isoforms in neurons of trigeminal ganglia

The abundance of 3-OST-2 and 3-OST-4 mRNA in trigeminal ganglion neurons was evaluated by real-time RT-PCR of neuron- or axon/Schwann cell-enriched samples obtained by laser capture microscopy (LCM) (Fig. 3A). Neuronal cell body samples exhibited strongest expression for 3-OST-2 and 3-OST-4 (Fig. 3B), with the ganglionic 3-OST-4 mRNA level being 20% of that for 3-OST-2. Of the remaining isoforms, 3-OST-1, 3-OST-3_B, and 3-OST-6 transcripts were detectable but at levels lower than that of 3-OST-4. It remains unclear whether these minor isoforms are expressed in neurons or contaminating satellite cells. In contrast to the neuron-enriched samples, the expression of all 3-OST isoforms was undetectable in the axonal/Schwann cell samples. Together with the above anatomical evidence, this quantitative transcript analysis demonstrates that 3-OST-2 and 3-OST-4 are the major 3-OST isoforms expressed in neurons of the trigeminal ganglion.

2.4. Isolation of the 3-OST-4 gene and cDNA

Before determining if products of 3-OST-2 and 3-OST-4 exist in neural tissues, we first needed to characterize the sulfation specificities of these enzymes. These analyses required functional cDNAs; however, only a partial length 3-OST-4 cDNA existed (Shworak et al., 1999). This limitation was circumvented by isolating the 3-OST-4 gene and appending a gene fragment to the available partial-length 3-OST-4 cDNA, thereby supplying the missing sequence. This technique is described and justified under the Experimental procedures.

The resultant full-length 3-OST-4 cDNA encoded a 49,825 Da protein with a type-II transmembrane topology (Fig. 4). The N-terminal region exhibits features common to most other 3-OST enzymes, including a short cytoplasmic tail, a hydrophobic membrane spanning segment, and a SPLAG domain (enriched in Ser, Pro, Leu, Ala, Gly) (Shworak et al., 1999). Similar to 3-OST-3_B, the 3-OST-4 cytoplasmic tail contains a polyproline stretch, which is thought to be a protein-protein interaction motif (Shworak et al., 1999). The C-terminal region encompasses a sulfotransferase domain that exhibits the greatest homology to 3-OST-2, 3-OST-3_A, and 3-OST-3_B isoforms (~76% identity). This high similarity in the sulfotransferase domain, suggests these enzymes may generate similar 3-*O*-sulfated structures.

2.5. Identification of 3-OST-2/4-type products in HS

The specificities of 3-OST-2 and 3-OST-4 were assessed by an established approach used to characterize the sulfation sites of 3-OST enzymes (Kuberan et al., 2002; Lawrence et al., 2004). We expressed each isoform in a cell line (CHO[Eco]) that normally does not express 3-OST enzymes (HajMohammadi et al., 2003). Retroviral expression constructs were employed so as to transduce >90% of cells (Chatterton et al., 1999; HajMohammadi et al., 2003). Cellular HS was degraded with heparinase I, II, and III (Hep I–III) under conditions that yield 3-*O*-sulfated disaccharides as well as digestion-resistant 3-*O*-sulfated tetrasaccharides (Yamada et al., 1993). The resulting digestion products were resolved by liquid chromatography/mass spectrometry (LC/MS). HS from non-transduced CHO[Eco] cells yielded only disaccharides containing *N*-, 2-*O*-, and/or 6-*O*-sulfates (Fig. 5). In addition to these residues, HS isolated from 3-OST transduced cells contained four 3-*O*-sulfated products (Fig. 5). Theses 3-OST-2/4-type digestion products were the disaccharides ΔUA2S→GlcNS**3S**, ΔUA2S→GlcNS**3S**6S (3-*O*-sulfate in bold), and two Hep I–III-resistant tetrasaccharides (Tetra-A and Tetra-B). Based on their molecular weights, the tetrasaccharides lack acetyl groups and contain 4 sulfate groups (Tetra-A, MW ~993) or 5 sulfate groups (Tetra-B, MW ~1073). We have previously found that 3-OST-3_A produces identical disaccharides and two tetrasaccharides of identical molecular weight to Tetra-A and Tetra-B (Lawrence et al., 2004), indicating that all three 3-OST enzymes exhibit, at the least, similar motif specificities.[6]

[5] Lawrence et al, unpublished data.

[6] We have ruled out that 3-OST-2 and 3-OST-4 function like 3-OST-5, which has a partially overlapping specificity (Lawrence et al., 2004). HS modified by any of these enzymes yields 3-OST-3_A-like products. However, 3-OST-5 modification also leads to high levels of 3-OST-1-type digestion products (ΔUA→GlcNS**3S** and ΔUA→GlcNS**3S**6S) (Xia et al., 2002). These signature disaccharides of HS^{AT+} are always found in near equimolar levels. Our chromatography system readily detects ΔUA→GlcNS**3S**6S (retention time of ~55 min), which exhibits baseline separation from ΔUA→GlcNS6S (retention time of ~57 min) (Lawrence et al., 2004). All Fig. 5 samples lack a peak in the ΔUA→GlcNS**3S**6S position. Moreover, water and DBA combine with ΔUA→GlcNS**3S**6S to form adducts with unique molecular masses (Lawrence et al., 2004); these distinctive molecular ions were not detected in our LC/MS analyses of 3-OST-2/4 digestion products (not shown). Thus, we conclude that 3-OST-2 and 3-OST-4 exhibit a distinct specificity from 3-OST-5, which produces substantial levels of 3-OST-1-type digestion products.

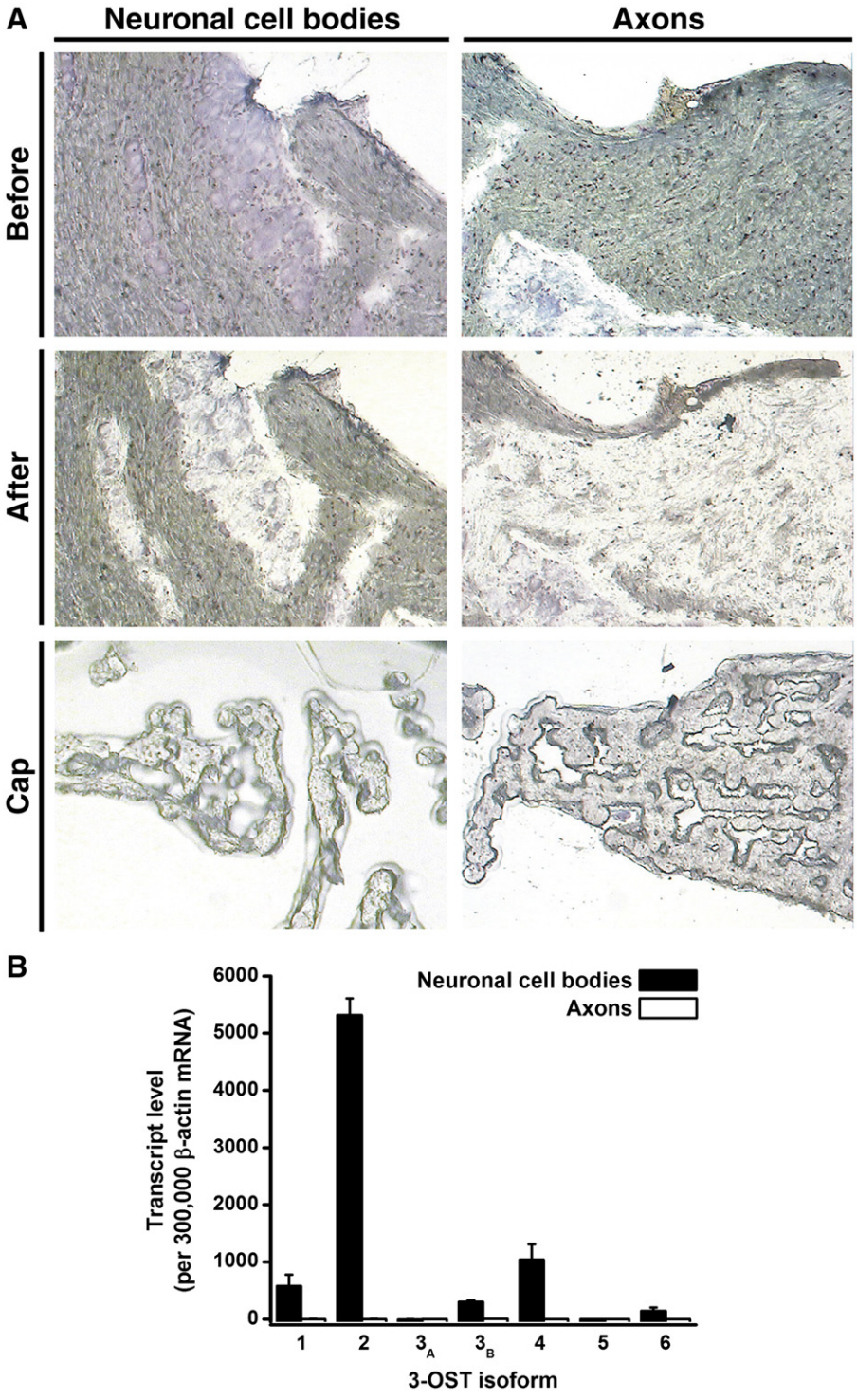

Fig. 3. 3-OST-2 and 3-OST-4 are the predominant 3-OST isoforms expressed by sensory neurons of the trigeminal ganglion. Individual sensory neurons with satellite cells (Neuronal cell bodies) or axonal processes with Schwann cells (Axons) were isolated from 8-μm cryosections of mouse trigeminal ganglia by LCM (Cap). Total RNA was extracted from samples containing approximately 100 neurons or 400 Schwann cells, then linearly amplified RNA was subjected to real-time RT-PCR, as described under Experimental procedures. (A) Hematoxylin and eosin stained sections (200×) before and after LCM, as indicated. For the neuronal samples, contaminating satellite cells comprised about 10% of the sample volume. (B) Expression of 3-OST isoforms in the indicated samples are the mean ± range from two independent cell isolations. Results are standardized to levels of β-actin.

2.6. Neural tissues expressing 3-OST-2 and 3-OST-4 exhibit 3-OST-2/4-type products

We examined three neural tissues for the specific HS products of 3-OST-2 and 3-OST-4. Tissue HS was digested with Hep I–III and liberated residues were identified by LC/MS. To provide the most definitive identification of the digestion products, we present spectra data that reveal the mass of relevant molecular ions. The 3-OST-2/4-type products are represented by a total of seven distinct molecular ions; however, for simplicity, we present

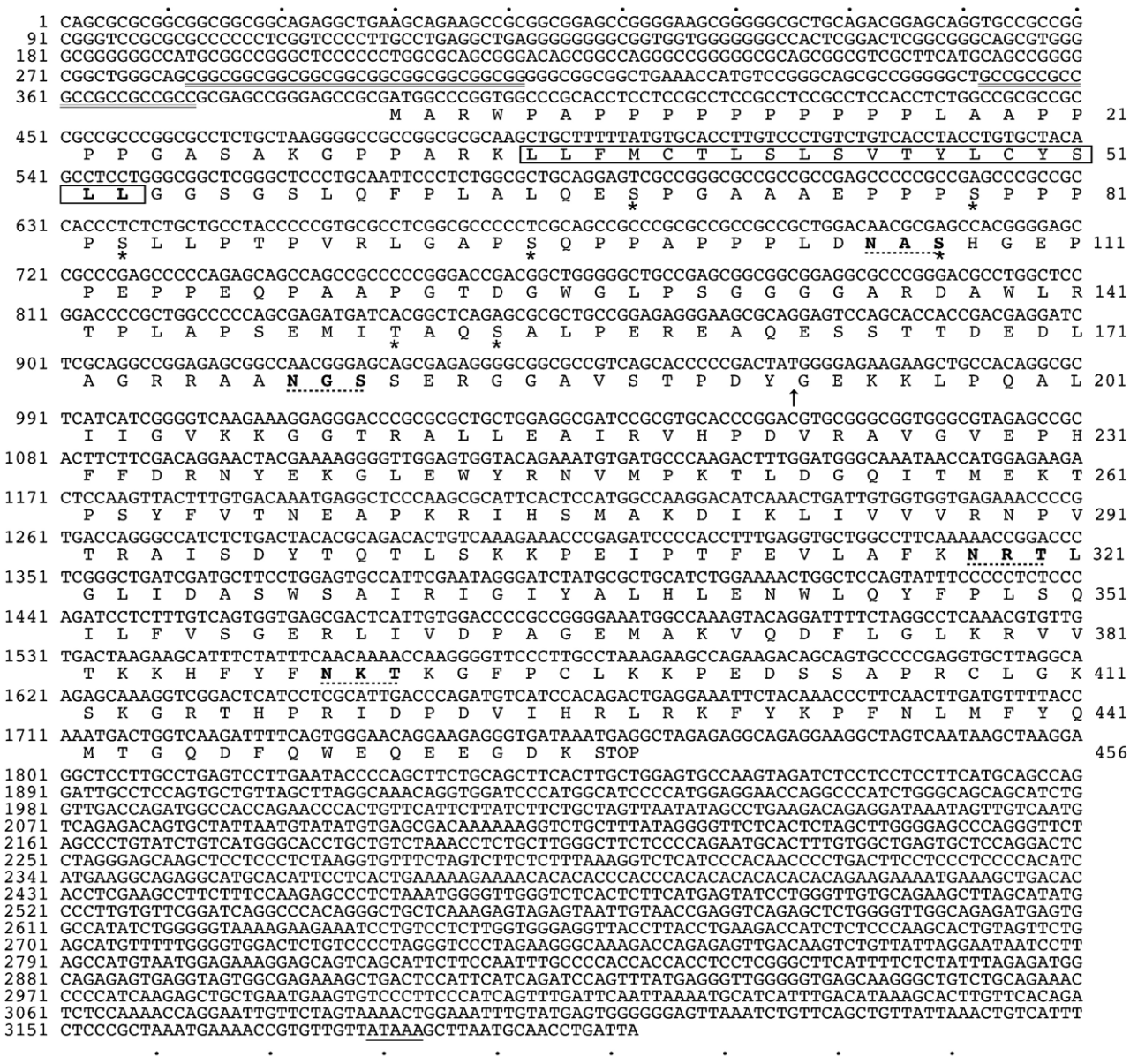

Fig. 4. Composite cDNA nucleotide and predicted amino acid sequences of human 3-OST-4. The cDNA sequence was compiled from overlapping genomic and cDNA sequences. Shown within the nucleic acid sequence are the polyadenylation signal (single underline) and a pure GC inverted repeat (double underline). Shown within the amino acid sequence are the transmembrane domain (boxed), the start of the sulfotransferase domain (arrow), and predicted sites for *O*-linked (*) and N-linked (dot underlined) glycosylation. Protein structural features were detected as previously described (Shworak et al., 1999). This sequence is GenBank accession number AF105378.

data for two diagnostic molecular ions—the $[M\text{-}2H+DBA]^{-1}$ form of the disaccharide ΔUA2S→GlcNS**3S**6S and the $[M\text{-}2H]^{-2}$ form of Tetra-B. Fig. 6 shows that 3-OST-2/4-type products were detectable in HS from the trigeminal ganglion and the brain stem but not the cerebellum.[7] In addition to the trigeminal ganglion, our *in situ* hybridizations revealed that 3-OST-2 and 3-OST-4 are also expressed in select neurons of the brain stem but not of the cerebellum[5]. Thus, 3-OST-2/4-type products were selectively detected in the tissues that express 3-OST-2 and 3-OST-4. We cannot rule out that some of these products are derived from synaptic projections of neurons from other regions; for example, trigeminal synaptic connections occur in the brain stem but not the cerebellum. Nevertheless, 3-OST-2 and 3-OST-4 are the major brain/neuronal 3-OST isoforms capable of making 3-OST-2/4-type products. Thus, the majority of such products detected in select neural tissues likely result from the selective expression of 3-OST-2 and 3-OST-4 in local and/or distant neurons.

[7] Despite our previous finding that brain HS^{AT+} is predominantly derived from 3-OST-1 (HajMohammadi et al., 2003), our LC/MS analysis did not detect ΔUA→GlcNS**3S**6S in neural HS samples. Our inability to detect this major 3-OST-1 digestion product is consistent with the rarity of 3-OST-1 derived disaccharides (<0.5% of sulfated disaccharides from cell lines expressing "high" levels of HS^{AT+}) (Colliec-Jouault et al., 1994; Shworak et al., 1994a). We conclude that in neural tissue, 3-OST-2/4-type 3-*O*-sulfated HS structures are far more abundant than 3-OST-1 modified residues.

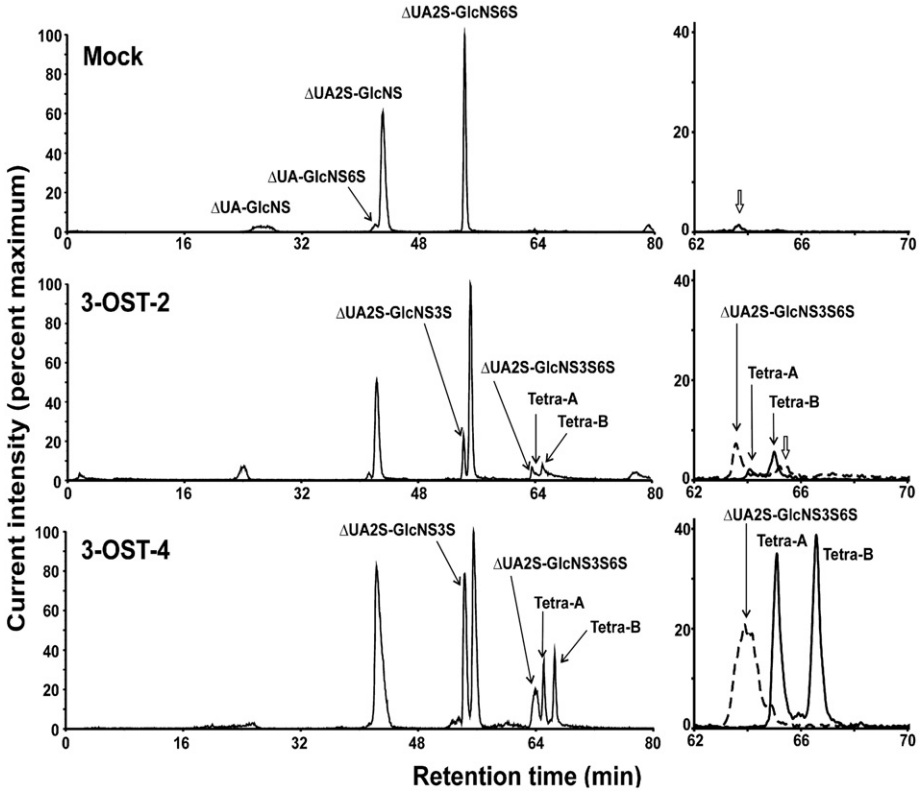

Fig. 5. Identification of 3-OST-2/4-type products. HS, extracted from CHO[Eco] cells transduced with empty retroviral vector (Mock) or vectors expressing the indicated enzymes, was digested with Hep I–III and the derived residues were subjected to LC/MS analysis, as described under Experimental procedures. Enzymatic cleavage converts GlcA/IdoA to ΔUA. For simplicity, the data are presented as the extracted ion current for sulfated HS saccharide residues only. Residues common to all chromatograms are indicated in the top (Mock) panel. 3-*O*-sulfated residues resulting from retroviral transduction are indicated in the 3-OST-2 and 3-OST-4 panels. Retention times varied slightly between duplicate runs of the same sample, so peak assignments were confirmed by their mass spectrographs (not shown), as we have previously described (Lawrence et al., 2004). Shown to the right are enlargements of the 62- to 70-min region with separate tracings indicating compounds having *m*/*z* values (±0.2 atomic mass units) consistent with sulfated tetrasaccharide residues (solid line) or the fully sulfated disaccharide, ΔUA2S→GlcNS**3S**6S (broken line). The open arrow indicates apparent contaminating species having *m*/*z* values inconsistent with but within the tolerance set for HS saccharide residues.

2.7. 3-OST-2 and 3-OST-4 mediate HSV-1 entry

Their similar motif specificities suggest that 3-OST-2, 3-OST-3_A, and 3-OST-4 may convey comparable cell biologic properties. Thus, we tested whether 3-OST-2 and 3-OST-4 function similarly to 3-OST-3_A or 3-OST-3_B, which we have shown generate HS^{gD+} that confers susceptibility to infection by HSV-1 (Shukla et al., 1999; Yabe et al., 2001). CHO cells, which are normally resistant to HSV-1, were transfected with plasmids expressing various 3-OSTs and then exposed to HSV-1(KOS)tk12—a recombinant HSV-1 strain that, upon entry into cells, expresses β-galactosidase. We found that expression of 3-OST-2 or 3-OST-4 was associated with enhanced susceptibility of the transfected cells to HSV-1 entry (Fig. 7), similar to that observed with the previously characterized 3-OST-3_A and 3-OST-3_B (Shukla et al., 1999; Yabe et al., 2001). These results conform with our prior finding that the conveyance of HSV-1 entry is dependent on the enzymatic specificity of the 3-OST isoform; as shown previously, the distinct 3-*O*-sulfated HS motifs generated by 3-OST-1 are unable to mediate HSV-1 entry (Shukla et al., 1999; Yabe et al., 2001).

3. Discussion

HS plays critical developmental and pathophysiological roles in the nervous system (Chipperfield et al., 2002; Ford-Perriss et al., 2002; Goedert et al., 1996; Hasegawa et al., 1997; Inatani et al., 2003; Irie et al., 2002; Kaksonen et al., 2002; Paudel and Li, 1999; Reizes et al., 2001; Yamaguchi, 2001). For example, HS of the extracellular matrix controls axonal guidance by modulating matrix signaling through receptors such as integrins (Bulow et al., 2002; Lee and Chien, 2004). However, the involvement of glucosamine 3-*O*-sulfation, which can regulate discrete HS activities, is presently unknown. To enable investigations into potential neural functions of this important HS modification, we sought to identify and characterize neuronal 3-OST isoforms. Our study reveals that 3-OST-2 and 3-OST-4 are major brain/neuronal 3-OST isoforms with properties that make them prime candidates for participating in HS-dependent neurobiologic events.

We first identified the major 3-OST isoforms expressed in the brain. Real-time PCR analyses demonstrated that in the mouse brain 3-OST-1, 3-OST-2 and 3-OST-4 are by far the most abundantly expressed isoforms. 3-OST-1 mRNA occurs in all

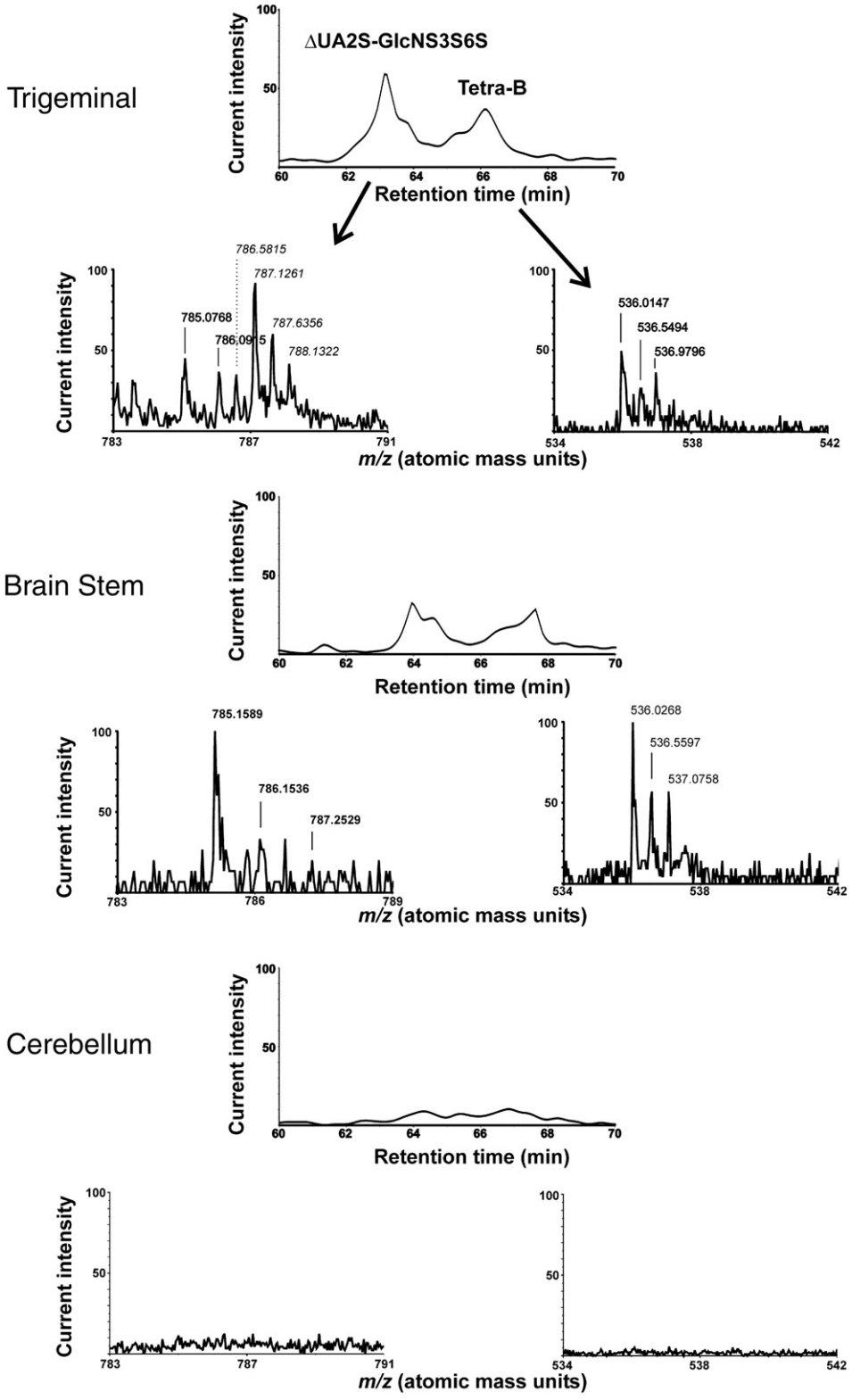

Fig. 6. 3-OST-2/4-type HS products occur in select neural tissues. LC/MS analysis of Hep I–III-digested HS extracted from the indicated mouse tissues. For simplicity we present data for two diagnostic molecular ions. The chromatograms show the extracted ion current for compounds having *m/z* values (±0.2 atomic mass units) consistent with ΔUA2S→GlcNS**3S**6S and Tetra B. Beneath are mass spectra for the $[M\text{-}2H+DBA]^{-1}$ form of ΔUA2S→GlcNS**3S**6S and the $[M\text{-}2H]^{-2}$ form of Tetra B. For the Tetra-B $[M\text{-}2H]^{-2}$ molecular ion (*m/z* of 536 atomic mass units), the −2 charge is confirmed by the isotopic cluster, which shows 0.5 atomic mass unit difference between adjacent peaks. For the ΔUA2S→GlcNS**3S**6S $[M\text{-}2H+DBA]^{-1}$ molecular ion (*m/z* of 785 atomic mass units), the isotopic cluster progresses by 1 atomic mass unit, indicating the charge of −1. The trigeminal sample also contains a contaminant (masses indicated in *italics*) co-eluting within the ΔUA2S→GlcNS**3S**6S region, which is distinguished by its *m/z* of 786.6 atomic mass units and its charge of −2 (peaks differing by 0.5 atomic mass units). The 787.1 peak likely contains signal from both the 3-*O*-sulfated disaccharide and the contaminant. For the cerebellum, the mass spectra corresponding to the elution ranges seen in both the trigeminal and the brain stem verified the absence of these species in cerebellar HS.

organs (HajMohammadi et al., 2003; Shworak et al., 1999); whereas 3-OST-2 and 3-OST-4 are preferentially expressed in the central nervous system (Shworak et al., 1999). Thus, we focused on these latter two major brain isoforms.

In situ hybridizations of brain and trigeminal ganglion demonstrated that 3-OST-2 and 3-OST-4 are both expressed predominantly, if not exclusively, in subpopulations of neurons. Our results do not rule out neuronal expression of other 3-OST isoforms; however, our *in situ* analyses combined with the quantitation of brain and trigeminal ganglion transcripts, indicate that 3-OST-2 and 3-OST-4 are the major 3-OST isoforms of neurons.

We addressed whether neuronal expression of 3-OST-2 and 3-OST-4 might affect the structure of neural HS. This process was enabled by our isolation of the 3-OST-4 gene, which provided the first full-length 3-OST-4 cDNA for identification of its enzymatic reaction products. LC/MS analysis of HS from transduced cells demonstrated that 3-OST-2 and 3-OST-4 catalyze similar, if not identical, modifications when resolved at the disaccharide and tetrasaccharide levels. Detectable levels of these 3-OST-2/4-type digestion products were only present in HS from neural tissues that express 3-OST-2 and 3-OST-4 (the trigeminal ganglion and brain stem, but not the cerebellum). On one hand, these data suggest that region specific expression of these isoforms may lead to region specific accumulation of 3-OST-2/4-type products. On the other hand, HSPGs generated by neurons can undergo axonal transport (Dow et al., 1994; Ripellino and Elam, 1988). Thus, 3-OST-2/4-type products generated in neuronal cell bodies may also be transported to their distant nerve endings. 3-OST-2 and 3-OST-4 expressing neurons may well have 3-OST-2/4-type products on axons and within synapses, as these structures contain HSPGs (Van Vactor et al., 2006). Moreover, modification of HSPGs occurs independent of the core protein (Shworak et al., 1994a,b; Zako et al., 2003);

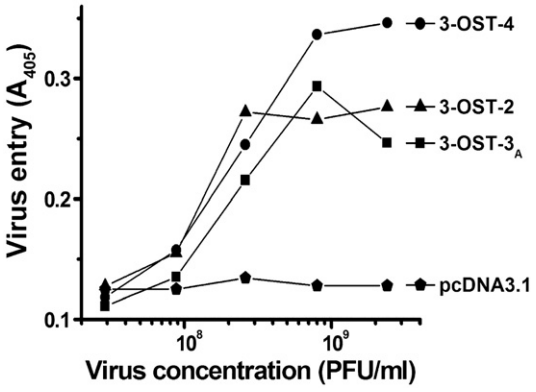

Fig. 7. 3-OST-2 and 3-OST-4 expression converts resistant CHO cells to susceptibility to HSV-1 entry. CHO cells were transfected with plasmids expressing the indicated 3-OST constructs or the empty vector (pcDNA3.1). Transfectants were exposed to serial dilutions of HSV-1(KOS)tk12, which expresses β-galactosidase from an insert in the viral genome. Viral entry-dependent β-galactosidase activity was quantitated at 6 h after the addition of virus, as described under Experimental procedures. Representative values from a single transfection show the amount of reaction product detected spectrophotometrically (A_{405}) as the mean from 3 wells per virus dose. Standard deviations were typically <15% of the mean. Comparable results were obtained in 5 independent transfection experiments.

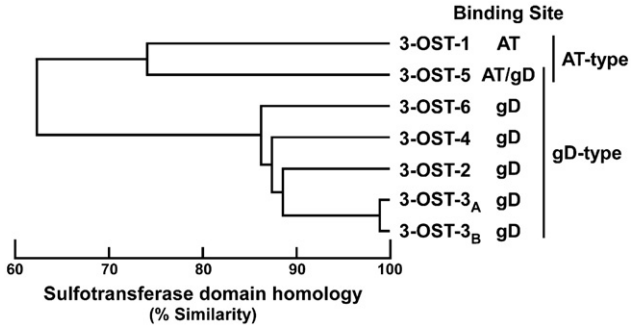

Fig. 8. The 3-OST multigene family is comprised of two structurally and functionally defined groups. The dendrogram of the human 3-OST multigene family shows the degree of sequence homology (% Similarity) within the previously defined sulfotransferase domain (Shworak et al., 1999; Yabe et al., 2001). Indicated are the preferred HS motifs generated by each enzyme, gD- or antithrombin (AT)-binding sites (Shukla et al., 1999; Shworak et al., 1996; Shworak et al., 1997; Xia et al., 2002; Xu et al., 2005, and data herein), and the resulting structural/functional categories. The dendrogram was generated with the University of Wisconsin Genetics Computer Group program "Distances" using amino acid sequences from GenBank/EMBL/DDBJ accession numbers: AF019386 (3-OST-1), AF105374 (3-OST-2), AF105376 (3-OST-3_A), AF105377 (3-OST-3_B), AF105378 (3-OST-4), AF50392 (3-OST-5), and AY574375 (3-OST-6).

thus, 3-OST expressing neurons should have 3-*O*-sulfated HS on their entire repertoire of core proteins, including synaptic HSPGs. Unfortunately, we presently cannot test this important hypothesis, which would require an as yet unavailable *in situ* probe that selectively binds to 3-OST-2/4-modified HS. Thus, it remains to be determined whether the detected 3-OST-2/4-type products are derived from local and/or distant neurons.[8] Regardless, it is most likely that the 3-*O*-sulfated HS products detected in select neural tissues are predominantly derived from 3-OST-2 and 3-OST-4, which are by far the major neuronal 3-OST isoforms that specifically generate such products.

The 3-OST-2/4-type products are also similar, if not identical, to disaccharide and tetrasaccharide products we have previously identified for 3-OST-3_A (Lawrence et al., 2004), suggesting that all three isoforms may regulate similar cellular processes. Indeed, we found that 3-OST-2 and 3-OST-4 mediate cellular entry of HSV-1 as previously shown for 3-OST-3_A and 3-OST-3_B, which generate HS^{gD+} for the HSV-1 receptor-binding glycoprotein, gD (Shukla et al., 1999). Thus, the comparable biochemical and viral entry data suggest that 3-OST-2 and 3-OST-4, like 3-OST-3_A and 3-OST-3_B, act by generating specific 3-*O*-sulfated sequences in HS that bind gD to trigger cellular entry of HSV-1.[9]

With the above characterizations, it is now apparent that the large 3-OST multigene family shows two major sequence specificities (Fig. 8). 3-OST-2, 3-OST-3_A, 3-OST-3_B, 3-OST-4, and 3-OST-6 (Shukla et al., 1999; Xu et al., 2005, and data herein) preferentially generate HS^{gD+} and so may be classified as gD-type enzymes. These isoforms show highly homologous sulfotransferase domains, consistent with this domain defining

[8] We have detected 3-OST-2/4-type products in trigeminal sensory fields; however, multiple cell types exist in these tissues so the cell types and 3-OST isoforms responsible for these products is entirely unclear.

[9] Indeed, evidence that 3-OST-2 and 3-OST-4 generate gD binding sites was recently published (Tiwari et al., 2005) while this manuscript was in preparation.

enzymatic sequence specificity (Yabe et al., 2001). The most structurally distinct enzyme, 3-OST-1, preferentially generates HS^{AT+} (Shworak et al., 1997) and is unable to convey susceptibility to HSV-1 cellular entry (Shukla et al., 1999; Yabe et al., 2001), so may be considered as an AT-type enzyme. 3-OST-5 exhibits both specificities (Xia et al., 2002), and must be considered a member of both classes. Thus, the majority of 3-OST isoforms can efficiently synthesize HS^{gD+}.

The full structure of the gD-binding motif has yet to be elucidated; however, a partial sequence has been proposed which encompasses the 3-OST-2/4-type product Tetra-B (Liu et al., 2002). Due to differing methods of analysis, it is not yet known whether all gD-type isoforms generate Tetra-B. Based on the known enzyme specificities (Kuberan et al., 2004; Liu et al., 1999a; Wu et al., 2004; Xia et al., 2002; Xu et al., 2005, and data herein), the minimum common structure produced by all gD-type isoforms is →IdoA2S→GlcN(S/H)**3S**±6S→; thus, this disaccharide motif is likely a key component of the gD-binding site. It remains to be determined whether individual gD-type isoforms generate structurally identical or distinct gD-binding sites.

Recent studies in *Drosophila melanogaster* suggest a critical role for the mammalian gD-type isoforms (Kamimura et al., 2004). *Drosophila* encodes only two 3-OST genes—*HS3ST-A* and *HS3ST-B*. The HS3ST-B enzyme is structurally most similar to the mammalian gD-type enzymes and its ectopic expression renders CHO cells susceptible to HSV-1 entry to the same extent as mammalian gD-type 3-OSTs (Kamimura et al., 2004). Gene silencing of *HS3ST-B* produces neurogenic phenotypes through cell autonomous inhibition of Notch signaling. HS3ST-B was found to act downstream of Notch transcription to enable accumulation of this receptor on the cell surface (Kamimura et al., 2004). Given the above structural and functional homologies, the mammalian gD-type isoforms may well serve to regulate cell surface levels of Notch receptors. Indeed among metazoans, Notch signaling components are extremely conserved (Artavanis-Tsakonas et al., 1999). During mammalian development, Notch receptors regulate cell fate by inhibiting neurogenesis and promoting gliogenesis (Grandbarbe et al., 2003). Notch signaling is additionally required for maintenance of neural stem cells (Artavanis-Tsakonas et al., 1999), which allow for neuron generation in sub-regions of the adult brain (Alvarez-Buylla and Lim, 2004). Mature neurons also express Notch isoforms, suggesting additional roles for these receptors in the adult nervous system (Irvin et al., 2001; Sestan et al., 1999). Given that 3-OST-2 and 3-OST-4 are major neuronal gD-type enzymes, they might be required for key Notch regulated events that determine cell fate in the developing and adult nervous system. A detailed analysis of this question is underway.

Our studies also suggest that of all gD-type isoforms, 3-OST-2 and 3-OST-4 are preferential candidates for involvement in HSV-1 infection of the nervous system. 3-OST-2 and 3-OST-4 are by far the most abundant gD-type isoforms in the central nervous system and so are likely the major source of neural 3-OST-2/4-type products. In particular, these isoforms are expressed in neurons of the trigeminal ganglion and perhaps other sensory ganglia, sites where HSV-1 establishes latent infections. However, it is presently unknown whether 3-*O*-sulfated HS occurs on nerve termini and is involved in HSV-1 infection of neurons. Moreover, there are additional cell surface receptors (herpesvirus entry mediator, and nectin-1) that can mediate HSV-1 infection of cultured cells (Cocchi et al., 1998; Geraghty et al., 1998; Montgomery et al., 1996; Warner et al., 1998). Of these, nectin-1 is also known to be expressed in neurons of the trigeminal ganglion (Haarr et al., 2001) and has been implicated in HSV-1 entry into cultured cells of neuronal origin (Manoj et al., 2004; Richart et al., 2003). Thus, more extensive studies will be required to evaluate whether *in vivo* HSV-1 infection involves 3-*O*-sulfated HS generated by neuronal gD-type 3-OSTs and/or the other candidate HSV-1 entry receptors.

Our identification of 3-OST-2 and 3-OST-4 as major neural gD-type 3-OSTs is a critical first step towards evaluating the involvement of neuronal 3-*O*-sulfated HS in the development and functioning of the central nervous system and in neuropathologies such as *in vivo* HSV-1 infection.

4. Experimental procedures

4.1. Cell lines and viruses

CHO-K1 (Esko et al., 1985) cells were cultured in Ham's F12 medium containing 10% fetal calf serum, 100 U/ml penicillin, 100 μg/ml streptomycin, and 2 mM glutamine. CHO [Eco] is a CHO-K1 derivative expressing the ecotropic retrovirus receptor (Gu et al., 2000). Phoenix cells (ATCC SD 3444) were grown in DMEM containing 10% fetal calf serum, 50 U/ml penicillin, 50 μg/ml streptomycin, and 2 mM glutamine. HSV-1(KOS)tk12 has been described elsewhere (Warner et al., 1998). The retroviral vector MVT-37 was prepared from the MSCVpac retroviral vector (Hawley et al., 1994) as described (Lawrence et al., 2004). The complete coding sequences for human clones of 3-OST-2 and 3-OST-4 were subcloned into appropriate restriction sites of MVT-37. The Phoenix packaging line was transfected with these 3-OST constructs by calcium phosphate, as previously described (Gu et al., 2000) and retroviral supernatants were snap frozen. CHO [Eco] cells were transduced as previously described (Gu et al., 2000) then selected with 7.5 μg/ml puromycin (Sigma-Aldrich, St. Louis, Missouri, USA).

4.2. Quantitation of 3-OST transcript levels by real-time RT-PCR

All animal experiments were performed following review and approval by Institutional Animal Care and Use Committees of Dartmouth and MIT, respectively. Brains were harvested from 4- to 5-month-old male and female mice (C57BL/6×129S4/SvJae F1 hybrids) and RNA was harvested by the TRI Reagent (Sigma-Aldrich, St. Louis, Missouri, USA) protocol. Real-time PCR was performed as previously described (Girardin et al., 2005). In brief, first strand synthesis of cDNA was performed with a mixture of eight primers specific to the 3′ untranslated regions of the target genes (β-actin and each 3-OST isoform). SYBR Green-based real-time PCR was then performed on

cDNA derived from 10 ng of total RNA. Pairs of β-actin or 3-OST isoform specific primers were targeted to unique sequences within the 3′ untranslated region using the program Primer Express (Applied Biosystems) and are described by HajMohammadi et al.[10] All PCR products were subjected to melting curve analysis to confirm amplification of a single anticipated target. All PCR products were cloned, sequence verified, and used to make quantitation standards that ranged from 1 million down to 200 copies per reaction. Results were expressed as 3-OST transcripts per 300,000 β-actin transcripts, which was the average β-actin level per PCR reaction.

4.3. In situ hybridization

Adult male mice (C57BL/6J), about 3 months old, were anesthetized by inhalation of isoflurane, then exsanguinated by incision of the inferior vena cava and perfusion of 6 ml of phosphate-buffered saline (PBS) through the left ventricle. Fixative (4% formaldehyde freshly prepared in PBS) was next perfused at 6 ml/min for 5 min, then at 2.75 ml/min for 30 min. Tissues were removed, immersed in the fixative for up to 12 h at 5 °C, subjected to dehydration, and embedded in paraffin. Sections of 5-μm thickness on microscope slides were stored at 5 °C.

Tissue sections were deparaffinized in xylene, rehydrated using a graded ethanol series (100% to 30%), rinsed in 150 mM NaCl and PBS, each for 5 min, and post-fixed in 4% formaldehyde in PBS for 30 min. Slides were treated with 20 μg/ml proteinase K (Roche Molecular Biochemicals, Indianapolis, Indiana, USA) in 50 mM Tris–HCl, pH 7.2, containing 5 mM EDTA at room temperature for 7.5 min and fixed in 4% formaldehyde in PBS. Acetylation was carried out for 10 min with 0.25% acetic anhydride in 100 mM triethanolamine, pH 8.0, and slides were rinsed sequentially in PBS and 150 mM NaCl, dehydrated through a graded ethanol series and allowed to dry at least 2 h prior to hybridization.

Probes were obtained by PCR from a murine brain cDNA library (CLONTECH Laboratories Inc., Palo Alto, California, USA). A 923-bp 3-OST-2 probe (GenBank accession number AY533705) was generated using PCR primers dTCGCTCTCCTGCACTTACCTGT and dGGATCAATCTGTACATGAGTTCTCCC which span nucleotides 78–1015 of the corresponding human 3-OST-2 coding sequence (GenBank accession number AF105374). A 235-bp 3-OST-4 probe (GenBank EST accession number BB311177) was isolated with the PCR primers dTCTCCAGACATCCTTTTCAAG and dAGGTTGCATTAAGCTTTATAAC. The cDNA fragments were inserted into pBluescript KS+ and sense or antisense riboprobes were synthesized with either T7 or T3 RNA polymerases from *Eco*RI or *Xho*I linearized plasmids, respectively, using a commercial kit (Promega, Madison WI) according to the manufacturer's instructions. Riboprobes were resuspended in 20 μl of 1 M DTT and 180 μl of hybridization buffer containing 20 mM Tris–HCl, pH 7.4, 5 mM EDTA, 10 mM Na_2HPO_4, 50% deionized formamide, 300 mM NaCl, 1× Denhardt's solution, 10% dextran sulfate, and 0.5 mg/ml of yeast total RNA.

Hybridization was carried out as previously described (Toselli et al., 1992). Briefly, tissue sections were overlaid with 30 μl of ^{35}S-labeled probes (25,000 cpm/μl in hybridization buffer) and 22×22 mm cover slips. Hybridization was carried out at 52 °C for 16 h in a humidified chamber. Slides were washed in 5× SSC with 10 mM DTT at 50 °C for 30 min and subsequently in 2× SSC, 50% formamide, and 10 mM DTT at 65 °C for 20 min. Slides were rinsed twice at 37 °C for 10 min in STE (10 mM Tris–HCl, pH 7.5, 400 mM NaCl, and 5 mM EDTA) then treated with RNase A (20 μg/ml) in STE at 37 °C for 45 min. Sections were washed with STE for 5 min, with 2× SSC for 15 min, and with 0.1× SSC for 15 min, each at 37 °C. Sections were dehydrated in an ethanol series (30–95%) in 0.3 M ammonium acetate and finally in 100% ethanol. Sections were coated in Kodak NTB-2 nuclear track emulsion and placed in a desiccation chamber for 8–10 weeks at 4 °C. Slides were developed in Kodak D-19 developer, stained with hematoxylin and eosin, and photographed using a Leitz Dialux 20 light microscope (Wetzlar, Germany).

4.4. LCM

Isoflurane-anesthetized male C57BL/6J mice were exsanguinated, as above but without perfusion or fixation, and trigeminal ganglia were removed and frozen in OCT and stored at −80 °C. Longitudinal sections (8-μm thickness) were mounted on glass slides. An Arcturus PixCell II laser-capture microdissection microscope was used to recover specific fields of either ganglion cell bodies or axons and their associated Schwann cells. The respective cell types were recovered from serial sections separated by 24 μm within the tissue. As per the manufacturer's instructions, RNA was extracted with a PicoPure RNA isolation kit (Arcturus Engineering Inc., Mountain View, California, USA) and subjected to two rounds of amplification with a RiboAmp RNA amplification kit (Arcturus Engineering Inc.). Amplified RNA samples were quantitated and monitored for quality with an Agilent 2100 Bioanalyzer using RNA 6000 Nano Chips (Agilent Technologies, Palo Alto, California, USA). Real-time PCR was conducted as above, except that during the first strand synthesis, the cRNA was primed with random hexamers. Results were standardized to levels of β-actin, which were comparable between neuronal and axonal groups.

4.5. Isolation and characterization of the HS3ST4 coding region

We had initially isolated a partial length human 3-OST-4 cDNA (GenBank accession number AF105378) (Shworak et al., 1999). We attempted recovering the missing coding sequences from brain mRNA samples by three separate approaches (screening a total brain cDNA library (Shworak et al., 1999), screening a primer extension cDNA library generated with a 3-OST-4 specific primer, and conducting 5′-RACE). These mRNA-based techniques were unsuccessful; consequently, genomic sequences were isolated. The primers 5′-dGCGCGCTGCTGGAGGCGAT and 5′-dGTCTTGGGCATCACATTTCTGTA were

[10] S. HajMohammadi, J. M. Rhodes, M. McNeely, P. G. Spear and N. W. Shworak, unpublished data.

used to amplify the cDNA nucleotides 14–134 (of AF105378). A human BAC library (Genome Systems Inc., St. Louis, Missouri, USA) was screened with the resulting probe and three independent genomic clones were detected. Separate *Eco*RI sub-libraries in pZerO-1 (Gibco Invitrogen, Grand Island, New York, USA) were generated from each, and re-screening identified clones containing an identical 4045 bp insert (GenBank accession number AY476736) containing the 5′ end of the HS3ST4 gene. Sequencing, as previously described (Shworak et al., 1997, 1999), revealed a single exon containing 734 bp of coding sequence that initiated with a strong Kozak sequence (Kozak, 1996). The 3′ end of this exon had 116 bp of overlap to the partial cDNA. Given that the cDNA overlapped with the first coding exon, a composite 3-OST-4 cDNA sequence was compiled with genomic nucleotides 2457 to 3579, which correspond to Fig. 4 composite nucleotides 1 to 1123, and with the partial cDNA (AF105378) representing nucleotides 1008 to 3201. The first 900 bp of the composite cDNA were exceedingly GC rich (70–87%); thereby accounting for the above difficulty in directly isolating a full-length cDNA. The composite cDNA predicts a 3-OST-4 transcript of ~3.2 kb, which corresponds well to the ~3.4 kb value we previously determined by Northern blot analysis (Shworak et al., 1999). This composite was confirmed by recently isolated expressed sequence tag clones. GenBank accession number AL834283 confirmed an additional 257 bp of overlap; whereas, GenBank accession number BI552211 shows overlap up to nucleotide 1 of the composite sequence.

4.6. Plasmid expression constructs

Expression plasmids containing human 3-OST-2 (pcDNA3-JL2.7) and 3-OST-3_A (pcDNA3-JL3.3) were described previously (Liu et al., 1999a; Shworak et al., 1997, 1999). A functional 3-OST-4 cDNA was generated using an *Eco*O109I site common to AF105378 and the genomic sequence. The 5′ untranslated region was removed as it exhibited a pure GC inverted repeat (Fig. 4) that might limit translation. The genomic coding region, preceded by a *Bam*HI site (underlined), was isolated by PCR with the primers 5′-dAAAA*GGATC-C*ATGGCCCGGTGGCCCGCACCTCCT and 5′-dTTTCT-GTACCACTCCAACCC. PCR was carried out with Taq Gold polymerase (PerkinElmer Life and Analytical Sciences Inc., Boston, Massachusetts, USA) by 20 cycles of 95 °C for 30 s, 58 °C for 45 s, and 75 °C for 1 min in 10% (v/v) dimethyl sulfoxide. The PCR product was cloned into PCR-Script Cam (Stratagene Inc., La Jolla, California, USA) then digested with *Eco*O109I and ligated to a 1.7-kb *Eco*O109I fragment of the partial cDNA (Shworak et al., 1999). The resulting complete 3-OST-4 coding region was subcloned into pcDNA3.1 as a 1.5-kb *Bam*HI fragment.

4.7. Isolation of cell and tissue HS

Confluent transduced CHO[Eco] cells (five 150-mm dishes) were washed with PBS then subjected to exhaustive proteolysis for 24 h at 37 °C in 120 ml digest buffer (0.17 mg/ml protease (EC 3.4.24.31, Sigma-Aldrich, St. Louis, Missouri, USA) in 40 mM sodium acetate, 320 mM sodium chloride, pH 6.5). The pooled supernatants were diluted 1.5× with water and applied to a 0.5 ml DEAE Sepharose (Pharmacia Biotech, Piscataway, New Jersey, USA) column, washed with 25 bed volumes of 250 mM sodium chloride, 20 mM sodium acetate, 0.02% weight/volume sodium azide, pH 6.0, and eluted with 2.5 ml of 1 M sodium chloride, 20 mM sodium acetate, pH 6.0. Polysaccharide chains were then precipitated with 10 ml 100% ethanol overnight at 4 °C and centrifuged at 2500×*g* for 10 min at 4 °C. Pellets were washed with 10 ml ice-cold 70% ethanol, re-centrifuged, air dried, dissolved in 0.1 to 0.2 ml sterile water, and stored at 4 °C until analyzed. Alternatively, tissues harvested from adult (3 months old) C57BL/6 mice were homogenized in PBS and HS was isolated as just described.

4.8. LC/MS analysis of Hep I–III-derived HS residues

HS preparations (about one third of the extracted HS mass in 10 μl) were combined with 82 μl of 24.4 mM ammonium acetate with 2 mM calcium acetate and 1 μl containing 0.33 mU each of Hep I–III (Seikagaku America Inc., Bethesda, MD, USA). Samples were digested for 16 h at 37 °C then lyophilized and reconstituted in 7 μl water plus 1 μl of ion pairing reagent dibutylamine (DBA) and subjected to LC/MS analysis, as previously described (Kuberan et al., 2002; Lawrence et al., 2004). In addition to the raw ionic weight for each residue, the combined weight for adduct ions formed with DBA was also analyzed. The extracted ion current was computed as described in the documentation for the Data Explorer software provided by Applied Biosystems (Foster City, CA, USA).

4.9. HSV-1 entry assay

Determination of CHO transfectant susceptibility to HSV-1 entry has been previously described (Montgomery et al., 1996; Shukla et al., 1999; Yabe et al., 2001). Briefly, subconfluent CHO-K1 cells in 6-well dishes were transfected with empty control vector or pcDNA3-based plasmids expressing one of the 3-OSTs (Yoon et al., 2003), using Lipofectamine (Gibco Invitrogen, Grand Island, New York, USA) according to the manufacturer's recommendations and 1.5 μg of plasmid DNA per well in 1 ml. At 24 h after transfection, the cells were replated in 96-well tissue culture dishes at $2–4\times10^4$ cells per well. About 16 h later, the cells were washed and exposed to serial dilutions of HSV-1(KOS)tk12 prepared in PBS containing glucose and 1% calf serum (100 μl of virus dilution per well in triplicate). Input multiplicities of infection ranged from about 10^2 to 10^4 PFU of virus per cell. It should be noted that the effective multiplicity of infection was about 1/1500 of these values, due to the fact that most input virus does not make contact with cells in small wells loaded with a large volume relative to the small monolayer surface area. After incubation with virus at 37 °C for 6 h, sufficient time to allow for viral entry and expression of viral genes, the cells were solubilized in 100 μl of PBS containing 0.5% NP-40 and the β-galactosidase substrate, *O*-nitro-phenyl β-D-galactopyranoside. Generation of the β-galactosidase product was monitored at 405 nm in a

Victor Wallac spectrophotometer (PerkinElmer Life and Analytical Sciences Inc., Boston, Massachusetts, USA).

Acknowledgments

We are grateful to members of the participating laboratories for their insightful comments. This work is supported in part by National Institutes of Health Grants PO1 HL41484-12 (RDR), R37 AI36293 (PGS), U19 AI31494 (PGS), RO1 AG023590 (NWS), and the Human Frontier Science Program grant RG0304 (NWS).

References

Alvarez-Buylla, A., Lim, D.A., 2004. For the long run: maintaining germinal niches in the adult brain. Neuron 41, 683–686.

Artavanis-Tsakonas, S., Rand, M.D., Lake, R.J., 1999. Notch signaling: cell fate control and signal integration in development. Science 284, 770–776.

Borjigin, J., Deng, J., Sun, X., De Jesus, M., Liu, T., Wang, M.M., 2003. Diurnal pineal 3-*O*-sulphotransferase 2 expression controlled by beta-adrenergic repression. J. Biol. Chem. 278, 16315–16319.

Bulow, H.E., Berry, K.L., Topper, L.H., Peles, E., Hobert, O., 2002. Heparan sulfate proteoglycan-dependent induction of axon branching and axon misrouting by the Kallmann syndrome gene *kal-1*. Proc. Natl. Acad. Sci. U. S. A. 99, 6346–6351.

Chatterton, J.E., Hirsch, D., Schwartz, J.J., Bickel, P.E., Rosenberg, R.D., Lodish, H.F., Krieger, M., 1999. Expression cloning of *LDLB*, a gene essential for normal Golgi function and assembly of the ldlCp complex. Proc. Natl. Acad. Sci. U. S. A. 96, 915–920.

Chipperfield, H., Bedi, K.S., Cool, S.M., Nurcombe, V., 2002. Heparan sulfates isolated from adult neural progenitor cells can direct phenotypic maturation. Int. J. Dev. Biol. 46, 661–670.

Cocchi, F., Menotti, L., Mirandola, P., Lopez, M., Campadelli-Fiume, G., 1998. The ectodomain of a novel member of the immunoglobulin subfamily related to the poliovirus receptor has the attributes of a bona fide receptor for herpes simplex virus types 1 and 2 in human cells. J. Virol. 72, 9992–10002.

Colliec-Jouault, S., Shworak, N.W., Liu, J., de Agostini, A.I., Rosenberg, R.D., 1994. Characterization of a cell mutant specifically defective in the synthesis of anticoagulantly active heparan sulfate. J. Biol. Chem. 269, 24953–24958.

Daniels, R.J., Peden, J.F., Lloyd, C., Horsley, S.W., Clark, K., Tufarelli, C., Kearney, L., Buckle, V.J., Doggett, N.A., Flint, J., Higgs, D.R., 2001. Sequence, structure and pathology of the fully annotated terminal 2 Mb of the short arm of human chromosome 16. Hum. Mol. Genet. 10, 339–352.

Dow, K.E., Levine, R.L., Solc, M.A., DaSilva, O., Riopelle, R.J., 1994. Axonal transport of proteoglycans in regenerating goldfish optic nerve. Exp. Neurol. 126, 129–137.

Esko, J.D., Lindahl, U., 2001. Molecular diversity of heparan sulfate. J. Clin. Invest. 108, 169–173.

Esko, J.D., Stewart, T.E., Taylor, W.H., 1985. Animal cell mutants defective in glycosaminoglycan biosynthesis. Proc. Natl. Acad. Sci. U. S. A. 82, 3197–3201.

Ford-Perriss, M., Guimond, S.E., Greferath, U., Kita, M., Grobe, K., Habuchi, H., Kimata, K., Esko, J.D., Murphy, M., Turnbull, J.E., 2002. Variant heparan sulfates synthesized in developing mouse brain differentially regulate FGF signaling. Glycobiology 12, 721–727.

Gallagher, J.T., 2001. Heparan sulfate: growth control with a restricted sequence menu. J. Clin. Invest. 108, 357–361.

Geraghty, R.J., Krummenacher, C., Cohen, G.H., Eisenberg, R.J., Spear, P.G., 1998. Entry of alphaherpesviruses mediated by poliovirus receptor-related protein 1 and poliovirus receptor. Science 280, 1618–1620.

Girardin, E.P., Hajmohammadi, S., Birmele, B., Helisch, A., Shworak, N.W., de Agostini, A.I., 2005. Synthesis of anticoagulantly active heparan sulfate proteoglycans by glomerular epithelial cells involves multiple 3-*O*-sulfotransferase isoforms and a limiting precursor pool. J. Biol. Chem. 280, 38059–38070.

Goedert, M., Jakes, R., Spillantini, M.G., Hasegawa, M., Smith, M.J., Crowther, R.A., 1996. Assembly of microtubule-associated protein tau into Alzheimer-like filaments induced by sulphated glycosaminoglycans. Nature 383, 550–553.

Grandbarbe, L., Bouissac, J., Rand, M., Hrabe de Angelis, M., Artavanis-Tsakonas, S., Mohier, E., 2003. Delta-Notch signaling controls the generation of neurons/glia from neural stem cells in a stepwise process. Development 130, 1391–1402.

Grobe, K., Inatani, M., Pallerla, S.R., Castagnola, J., Yamaguchi, Y., Esko, J.D., 2005. Cerebral hypoplasia and craniofacial defects in mice lacking heparan sulfate *Ndst1* gene function. Development 132, 3777–3786.

Gu, X., Lawrence, R., Krieger, M., 2000. Dissociation of the high density lipoprotein and low density lipoprotein binding activities of murine scavenger receptor class B type I (mSR-BI) using retrovirus library-based activity dissection. J. Biol. Chem. 275, 9120–9130.

Haarr, L., Shukla, D., Rodahl, E., Dal Canto, M.C., Spear, P.G., 2001. Transcription from the gene encoding the herpesvirus entry receptor nectin-1 (HveC) in nervous tissue of adult mouse. Virology 287, 301–309.

HajMohammadi, S., Enjyoji, K., Princivalle, M., Christi, P., Lech, M., Beeler, D., Rayburn, H., Schwartz, J.J., Barzegar, S., de Agostini, A.I., Post, M.J., Rosenberg, R.D., Shworak, N.W., 2003. Normal levels of anticoagulant heparan sulfate are not essential for normal hemostasis. J. Clin. Invest. 111, 989–999.

Hasegawa, M., Crowther, R.A., Jakes, R., Goedert, M., 1997. Alzheimer-like changes in microtubule-associated protein Tau induced by sulfated glycosaminoglycans. Inhibition of microtubule binding, stimulation of phosphorylation, and filament assembly depend on the degree of sulfation. J. Biol. Chem. 272, 33118–33124.

Hawley, R.G., Lieu, F.H., Fong, A.Z., Hawley, T.S., 1994. Versatile retroviral vectors for potential use in gene therapy. Gene Ther. 1, 136–138.

Inatani, M., Irie, F., Plump, A.S., Tessier-Lavigne, M., Yamaguchi, Y., 2003. Mammalian brain morphogenesis and midline axon guidance require heparan sulfate. Science 302, 1044–1046.

Iozzo, R.V., 2001. Heparan sulfate proteoglycans: intricate molecules with intriguing functions. J. Clin. Invest. 108, 165–167.

Iozzo, R.V., San Antonio, J.D., 2001. Heparan sulfate proteoglycans: heavy hitters in the angiogenesis arena. J. Clin. Invest. 108, 349–355.

Irie, A., Yates, E.A., Turnbull, J.E., Holt, C.E., 2002. Specific heparan sulfate structures involved in retinal axon targeting. Development 129, 61–70.

Irvin, D.K., Zurcher, S.D., Nguyen, T., Weinmaster, G., Kornblum, H.I., 2001. Expression patterns of Notch1, Notch2, and Notch3 suggest multiple functional roles for the Notch-DSL signaling system during brain development. J. Comp. Neurol. 436, 167–181.

Kaksonen, M., Pavlov, I., Voikar, V., Lauri, S.E., Hienola, A., Riekki, R., Lakso, M., Taira, T., Rauvala, H., 2002. Syndecan-3-deficient mice exhibit enhanced LTP and impaired hippocampus-dependent memory. Mol. Cell Neurosci. 21, 158–172.

Kamimura, K., Rhodes, J.M., Ueda, R., McNeely, M., Shukla, D., Kimata, K., Spear, P.G., Shworak, N.W., Nakato, H., 2004. Regulation of Notch signaling by *Drosophila* heparan sulfate 3-*O* sulfotransferase. J. Cell Biol. 166, 1069–1079.

Kozak, M., 1996. Interpreting cDNA sequences: some insights from studies on translation. Mamm. Genome 7, 563–574.

Kuberan, B., Lech, M., Zhang, L., Wu, Z.L., Beeler, D.L., Rosenberg, R.D., 2002. Analysis of heparan sulfate oligosaccharides with ion pair-reverse phase capillary high performance liquid chromatography-microelectrospray ionization time-of-flight mass spectrometry. J. Am. Chem. Soc. 124, 8707–8718.

Kuberan, B., Lech, M., Borjigin, J., Rosenberg, R.D., 2004. Light-induced 3-*O*-sulfotransferase expression alters pineal heparan sulfate fine structure. A surprising link to circadian rhythm. J. Biol. Chem. 279, 5053–5054.

Lawrence, R., Kuberan, B., Lech, M., Beeler, D.L., Rosenberg, R.D., 2004. Mapping critical biological motifs and biosynthetic pathways of heparan sulfate. Glycobiology 14, 467–479.

Lee, J.S., Chien, C.B., 2004. When sugars guide axons: insights from heparan sulphate proteoglycan mutants. Nat. Rev., Genet. 5, 923–935.

Liu, J., Shworak, N.W., Fritze, L.M., Edelberg, J.M., Rosenberg, R.D., 1996. Purification of heparan sulfate D-glucosaminyl 3-*O*-sulfotransferase. J. Biol. Chem. 271, 27072–27082.

Liu, J., Shriver, Z., Blaiklock, P., Yoshida, K., Sasisekharan, R., Rosenberg, R.D., 1999a. Heparan sulfate D-glucosaminyl 3-*O*-sulfotransferase-3$_A$ sulfates *N*-unsubstituted glucosamine residues. J. Biol. Chem. 274, 38155–38162.

Liu, J., Shworak, N.W., Sinay, P., Schwartz, J.J., Zhang, L., Fritze, L.M., Rosenberg, R.D., 1999b. Expression of heparan sulfate D-glucosaminyl 3-*O*-sulfotransferase isoforms reveals novel substrate specificities. J. Biol. Chem. 274, 5185–5192.

Liu, J., Shriver, Z., Pope, R.M., Thorp, S.C., Duncan, M.B., Copeland, R.J., Raska, C.S., Yoshida, K., Eisenberg, R.J., Cohen, G., Linhardt, R.J., Sasisekharan, R., 2002. Characterization of a heparan sulfate octasaccharide that binds to herpes simplex virus type 1 glycoprotein D. J. Biol. Chem. 277, 33456–33467.

Manoj, S., Jogger, C.R., Myscofski, D., Yoon, M., Spear, P.G., 2004. Mutations in herpes simplex virus glycoprotein D that prevent cell entry via nectins and alter cell tropism. Proc. Natl. Acad. Sci. U. S. A. 101, 12414–12421.

McKeehan, W.L., Wu, X., Kan, M., 1999. Requirement for anticoagulant heparan sulfate in the fibroblast growth factor receptor complex. J. Biol. Chem. 274, 21511–21514.

Mochizuki, H., Yoshida, K., Gotoh, M., Sugioka, S., Kikuchi, N., Kwon, Y.D., Tawada, A., Maeyama, K., Inaba, N., Hiruma, T., Kimata, K., Narimatsu, H., 2003. Characterization of a heparan sulfate 3-*O*-sulfotransferase-5, an enzyme synthesizing a tetrasulfated disaccharide. J. Biol. Chem. 278, 26780–26787.

Montgomery, R.I., Warner, M.S., Lum, B.J., Spear, P.G., 1996. Herpes simplex virus-1 entry into cells mediated by a novel member of the TNF/NGF receptor family. Cell 87, 427–436.

Paudel, H.K., Li, W., 1999. Heparin-induced conformational change in microtubule-associated protein Tau as detected by chemical cross-linking and phosphopeptide mapping. J. Biol. Chem. 274, 8029–8038.

Reizes, O., Lincecum, J., Wang, Z., Goldberger, O., Huang, L., Kaksonen, M., Ahima, R., Hinkes, M.T., Barsh, G.S., Rauvala, H., Bernfield, M., 2001. Transgenic expression of syndecan-1 uncovers a physiological control of feeding behavior by syndecan-3. Cell 106, 105–116.

Richart, S.M., Simpson, S.A., Krummenacher, C., Whitbeck, J.C., Pizer, L.I., Cohen, G.H., Eisenberg, R.J., Wilcox, C.L., 2003. Entry of herpes simplex virus type 1 into primary sensory neurons in vitro is mediated by Nectin-1/HveC. J. Virol. 77, 3307–3311.

Ripellino, J.A., Elam, J.S., 1988. Axonal transport of proteoglycans to the goldfish optic tectum. Neurochem. Res. 13, 479–485.

Rosenberg, R.D., Shworak, N.W., Liu, J., Schwartz, J.J., Zhang, L., 1997. Heparan sulfate proteoglycans of the cardiovascular system. Specific structures emerge but how is synthesis regulated? J. Clin. Invest. 99, 2062–2070.

Sasisekharan, R., Shriver, Z., Venkataraman, G., Narayanasami, U., 2002. Roles of heparan-sulphate glycosaminoglycans in cancer. Nat. Rev., Cancer 2, 521–528.

Schmutzhard, E., 2001. Viral infections of the CNS with special emphasis on herpes simplex infections. J. Neurol. 248, 469–477.

Shukla, D., Spear, P.G., 2001. Herpesviruses and heparan sulfate: an intimate relationship in aid of viral entry. J. Clin. Invest. 108, 503–510.

Shukla, D., Liu, J., Blaiklock, P., Shworak, N.W., Bai, X., Esko, J.D., Cohen, G.H., Eisenberg, R.J., Rosenberg, R.D., Spear, P.G., 1999. A novel role for 3-*O*-sulfated heparan sulfate in herpes simplex virus 1 entry. Cell 99, 13–22.

Sestan, N., Artavanis-Tsakonas, S., Rakic, P., 1999. Contact-dependent inhibition of cortical neurite growth mediated by notch signaling. Science 286, 741–746.

Shworak, N.W., 2001. Selective detection of sulfotransferase isoforms by the ligand affinity-conversion approach. Methods Mol. Biol. 171, 91–101.

Shworak, N.W., Rosenberg, R.D., 1995. Antithrombotic defense potential of the blood vessel wall: the heparan sulfate-antithrombin pathway, pp. 119–146. In J.R. Vane, G.V.R. Born, and D. Welzel (eds.), The endothelial cell in health and disease, Schattauer, Stuttgart. pp. 119–146.

Shworak, N.W., Shirakawa, M., Colliec-Jouault, S., Liu, J., Mulligan, R.C., Birinyi, L.K., Rosenberg, R.D., 1994a. Pathway-specific regulation of the synthesis of anticoagulantly active heparan sulfate. J. Biol. Chem. 269, 24941–24952.

Shworak, N.W., Shirakawa, M., Mulligan, R.C., Rosenberg, R.D., 1994b. Characterization of ryudocan glycosaminoglycan acceptor sites. J. Biol. Chem. 269, 21204–21214.

Shworak, N.W., Fritze, L.M., Liu, J., Butler, L.D., Rosenberg, R.D., 1996. Cell-free synthesis of anticoagulant heparan sulfate reveals a limiting activity which modifies a nonlimiting precursor pool. J. Biol. Chem. 271, 27063–27071.

Shworak, N.W., Liu, J., Fritze, L.M., Schwartz, J.J., Zhang, L., Logeart, D., Rosenberg, R.D., 1997. Molecular cloning and expression of mouse and human cDNAs encoding heparan sulfate D-glucosaminyl 3-*O*-sulfotransferase. J. Biol. Chem. 272, 28008–28019.

Shworak, N.W., Liu, J., Petros, L.M., Zhang, L., Kobayashi, M., Copeland, N.G., Jenkins, N.A., Rosenberg, R.D., 1999. Multiple isoforms of heparan sulfate D-glucosaminyl 3-*O*-sulfotransferase. Isolation, characterization, and expression of human cDNAs and identification of distinct genomic loci. J. Biol. Chem. 274, 5170–5184.

Spear, P.G., Eisenberg, R.J., Cohen, G.H., 2000. Three classes of cell surface receptors for alphaherpesvirus entry. Virology 275, 1–8.

Tiwari, V., O'Donnell, C.D., Oh, M.J., Valyi-Nagy, T., Shukla, D., 2005. A role for 3-*O*-sulfotransferase isoform-4 in assisting HSV-1 entry and spread. Biochem. Biophys. Res. Commun. 338, 930–937.

Toselli, P., Faris, B., Sassoon, D., Jackson, B.A., Franzblau, C., 1992. In-situ hybridization of tropoelastin mRNA during the development of the multilayered neonatal rat aortic smooth muscle cell culture. Matrix 12, 321–332.

Van Vactor, D., Wall, D.P., Johnson, K.G., 2006. Heparan sulfate proteoglycans and the emergence of neuronal connectivity. Curr. Opin. Neurobiol. 16, 40–51.

Warner, M.S., Geraghty, R.J., Martinez, W.M., Montgomery, R.I., Whitbeck, J.C., Xu, R., Eisenberg, R.J., Cohen, G.H., Spear, P.G., 1998. A cell surface protein with herpesvirus entry activity (HveB) confers susceptibility to infection by mutants of herpes simplex virus type 1, herpes simplex virus type 2, and pseudorabies virus. Virology 246, 179–189.

Wu, Z.L., Lech, M., Beeler, D.L., Rosenberg, R.D., 2004. Determining heparan sulfate structure in the vicinity of specific sulfotransferase recognition sites by mass spectrometry. J. Biol. Chem. 279, 1861–1866.

Xia, G., Chen, J., Tiwari, V., Ju, W., Li, J.P., Malmstrom, A., Shukla, D., Liu, J., 2002. Heparan sulfate 3-*O*-sulfotransferase isoform 5 generates both an antithrombin-binding site and an entry receptor for herpes simplex virus, type 1. J. Biol. Chem. 277, 37912–37919.

Xu, D., Tiwari, V., Xia, G., Clement, C., Shukla, D., Liu, J., 2005. Characterization of heparan sulphate 3-*O*-sulphotransferase isoform 6 and its role in assisting the entry of herpes simplex virus type 1. Biochem. J. 385, 451–459.

Yabe, T., Shukla, D., Spear, P.G., Rosenberg, R.D., Seeberger, P.H., Shworak, N.W., 2001. Portable sulphotransferase domain determines sequence specificity of heparan sulphate 3-*O*-sulphotransferases. Biochem. J. 359, 235–241.

Yamada, S., Yoshida, K., Sugiura, M., Sugahara, K., Khoo, K.H., Morris, H.R., Dell, A., 1993. Structural studies on the bacterial lyase-resistant tetrasaccharides derived from the antithrombin III-binding site of porcine intestinal heparin. J. Biol. Chem. 268, 4780–4787.

Yamaguchi, Y., 2001. Heparan sulfate proteoglycans in the nervous system: their diverse roles in neurogenesis, axon guidance, and synaptogenesis. Semin. Cell Dev. Biol. 12, 99–106.

Ye, S., Luo, Y., Lu, W., Jones, R.B., Linhardt, R.J., Capila, I., Toida, T., Kan, M., Pelletier, H., McKeehan, W.L., 2001. Structural basis for interaction of FGF-1, FGF-2, and FGF-7 with different heparan sulfate motifs. Biochemistry 40, 14429–14439.

Yoon, M., Zago, A., Shukla, D., Spear, P.G., 2003. Mutations in the N termini of herpes simplex virus type 1 and 2 gDs alter functional interactions with the entry/fusion receptors HVEM, nectin-2, and 3-*O*-sulfated heparan sulfate but not with nectin-1. J. Virol. 77, 9221–9231.

Zako, M., Dong, J., Goldberger, O., Bernfield, M., Gallagher, J.T., Deakin, J.A., 2003. Syndecan-1 and-4 synthesized simultaneously by mouse mammary gland epithelial cells bear heparan sulfate chains that are apparently structurally indistinguishable. J. Biol. Chem. 278, 13561–13569.